NASA TECHNICAL MEMORANDUM

NASA TM X-71825

NASA TM X-71825

COMBINED-LOAD STRESS-STRAIN RELATIONSHIPS FOR ADVANCED FIBER COMPOSITES

by C. C. Chamis and T. L. Sullivan
Lewis Research Center
Cleveland, Ohio 44135

TECHNICAL PAPER to be presented at
Thirty-first Annual Reinforced Plastics Composites Conference sponsored by the Society of the Plastics Industry
Washington, D. C., February 3-6, 1976

CONTENTS

COMBINED-LOAD STRESS-STRAIN RELATIONSHIPS FOR ADVANCED FIBER COMPOSITES

by C. C Chamis and T. L. Sullivan
Lewis Research Center

ABSTRACT

It was demonstrated experimentally that only one test specimen is required to determine the combined-load stress-strain relationships of a given fiber composite system. These relationships were determined using a thin angle-plied laminate tube and subjecting it to a number of combined-loading conditions. The measured data obtained are compared with theoretical predictions. Also, some important considerations associated with such a test are identified, and the significance of combined-load stress-strain relationships in certain practical designs are discussed.

E-8526

INTRODUCTION

Composite structural components are required to resist a multitude of combined-load conditions in general. Therefore, combined-load stress-strain relationships are important in studying the structural response of a component, in setting design limit stresses and strains, and in correlating theoretical predictions with measured data. Since the combined stress-strain relationships may be measured without fracturing the specimen, it becomes both economical and expedient to use only one specimen in such tests. However, for generating design data, the statistical variation within the material population may require the use of more than one specimen.

Several test methods have been devised to test fiber composites under uniaxial and combined loading, reference 1. However, the possibility of

subjecting only one specimen to a multitude of combined loading conditions and measuring the corresponding response (stress-strain-behavior) to allow prediction of the behavior for any combined-loading condition has not been demonstrated. Therefore, the primary objective of this investigation was to demonstrate that only one test specimen is needed to determine the combined-load stress-strain relations of a fiber composite laminate. Additional objectives were: evaluation of these relations under a multitude of combined-loading conditions, correlation of measured data with laminate theory predictions, identification of possible difficulties associated with such tests, and determination of possible implications for practical design applications. The approach used to achieve the objectives of this investigation included the study of both experimental and theoretical aspects of the problem.

In this report, combined-load stress-strain relationships, combined-load elastic constants (coefficients) and combined-load apparent stiffness are used interchangeably in the text.

EXPERIMENTAL PROGRAM

The experimental program of this investigation consisted of fabricating and instrumenting the thin composite tube test specimen, preparing it for combined-load testing, testing, data acquisition, and data reduction. These steps are described in detail in the following sections. The multiaxial testing machine used to test the tubes, the data acquisition system, and the automated data reduction procedure are discussed briefly.

Specimen Fabrication and Instrumentation

The tubular specimen was fabricated using 4 mil diameter boron fiber and ERLA 4617/MPDA epoxy resin. The ply layup was $\left[(\pm 45)_2\right]_s$.

Between each boron/epoxy ply was a layer of fiber glass scrim cloth (used primarily as a carrier material). The nominal fiber volume content was 0.50. The nominal properties of the unidirectional composite are summarized in Table I.

The specimen was 12-inches long and had an inside diameter of 2.00-inches. The wall thickness was approximately 0.043-inch. The specimen was instrumented with three delta-rosettes with one element of each rosette aligned with the longitudinal axis of the tube. They were located 90^{o} apart at the midlength of the tube. A schematic of the composite tube specimen showing instrumentation and loads is shown in figure 1.

Testing Procedure

The specimen was tested in the NASA-Lewis Multiaxial Testing Facility. Figure 2 is a photograph of this facility. The facility consists of a multiaxial loading frame, hydraulic power supply (remotely located), control console, 32 channels of strain gage conditioning, and data recording instrumentation. The loading frame has the capability of applying axial tension or compression loads up to 100 000 pounds, torque up to 50 000 inch-pounds, and pressure up to 20 000 psi. Loads are servo controlled and can be applied individually, simultaneously, or sequentially. Compensation for axial stress due to pressure can be programmed by addition of axial compression.

Prior to testing, the inside of the specimen was coated with a thin (0.005-inch) layer of a urethane resin to prevent leaking of the pressurizing fluid through the tube wall; the specimen was then potted into metal

grips using an epoxy resin. Figure 3(a) provides a photograph of a tube specimen and grips mounted in the testing machine.

Testing was conducted as follows: Load command signals were obtained from one or two ramp generators depending on the type of loading required. For tests where combined-loading was required, the load ratio to give the desired stress ratio was calculated. Loading was halted at convenient intervals in order to obtain strain gage recordings. In some cases the stress ratio was not exactly as desired, or varied slightly during the test. This was caused by small nonlinearities in the controls, initialization at not exactly zero, and slight differences in loading speed when it was necessary to use two ramp generators. Strain gage and load data were reduced using the computer program described in reference 2. Except for the last test, maximum load levels were kept low enough to avoid damaging the tube. A photograph of the fractured tube specimen is shown in figure 3(b).

Experimental Results and Discussion

The experimental results pertinent to the present investigation consist of the composite or laminate stresses (tube wall average stress) and the corresponding axial, hoop, and shear strains measured as noted in figure 1. Terminal (maximum) stress, stress-strain curves and the combined-load stress-strain relationships (combined-load apparent stiffness) are obtained from the stress-strain results.

For the sake of brevity, the results from only a single rosette will be presented and discussed. To give the reader some idea of the variation among the rosettes around the circumference the results for all three rosettes for one load condition only will also be presented.

Terminal stresses. - The terminal (maximum) stresses at each combined load condition are summarized in Table II. Note the nominal loading-condition combinations are given in the first three columns. The actual composite (laminate) stresses are given under the appropriate column headings - axial, hoop, or torsional. Note also that for the final test the specimen was loaded to fracture in the combined loading condition (1:0:1.2) (last entry in Table II).

The important point to be observed from the results in Table II is that the nominal combined-loading condition desired (first three columns) was closely approximated by the actual stresses during testing.

Stress-strain curves. - Stress-strain curves for various single and combined-loading conditions were plotted via the computer, as follows, (refer to fig. 1):

1. axial stress versus axial strain ($\sigma_{cxx}/\epsilon_{cxx}$)
2. hoop stress versus hoop strain ($\sigma_{cyy}/\epsilon_{cyy}$)
3. shear stress versus shear strain ($\sigma_{cxy}/\epsilon_{cxy}$)
4. hoop strain versus axial strain ($\epsilon_{cyy}/\epsilon_{cxx}$)
5. shear strain versus axial strain ($\epsilon_{cxy}/\epsilon_{cxx}$)

The notation introduced above is as follows: σ denotes stress and ϵ denotes strain; the subscript c denotes composite, laminate, or tube wall for the present case; subscripts x and y denote coordinate directions (the first defines the normal to the plane on which σ or ϵ act and the second defines the direction of σ or ϵ). Note that some loading conditions, such as axial stress only, will not generate data for all five stress-strain curves defined above.

For convenience, the stress-strain curves from one loading condition are given in the general caption of each figure; the loading condition is noted in the caption. For example, the combined-loading axial tension with internal pressure (hoop tension) is noted thus: "Combined load stress ratio: (1:1:0)." The particular type stress-strain curve (types 1 to 5 above) are called out by sub-captions.

Stress-strain curves for uniaxial loadings are shown, respectively: axial tension, figure 4; axial compression, figure 5; hoop tension, figure 6; and torsion, figure 7. The collective points to be noted from figures 4 to 7 are:

1. The stress-strain curves for axial stress, hoop stress, shear stress and the corresponding Poisson's strains ($\epsilon_{cyy}/\epsilon_{cxx}$) are linear in the range tested.

2. The shear strain, ($\epsilon_{cxy}/\epsilon_{cxx}$) figures 4(c) and 5(c), is small compared to Poisson strain, ($\epsilon_{cyy}/\epsilon_{cxx}$). This small amount of shear strain could be caused by the following factors: testing machine normal-shear load cross-talk, small load eccentricities, small ply misorientations, strain gage misalignment, or a combination of these.

Combined load stress-strain curves for axial tension with transverse tension (1:1:0) are shown in figure 8. As can be observed, the stress strain curves in figure 8 are generally linear.

Corresponding stress-strain curves for axial compression with transverse tension (-1:1:0) are shown in figure 9. Note in this figure that both the axial and hoop stress-strain curves are nonlinear. It is believed that this nonlinearity arises because the combined loading

condition stresses the plies in the nonlinear region of the ply intralaminar shear stress-strain curve. More will be said about this in the theoretical portion of this report. Note also that the hoop strain curve (Poisson effect), figure 9(c), is linear. Furthermore, there is some shear strain, figure 9(d), which could be caused by factors already mentioned; however, it should be noted that it is an order of magnitude less than the axial strain.

Combined-load stress-strain curves for axial tension with torsion (shear) (1:0:1) are shown in figure 10. As can be observed from figure 10, all the stress-strain curves are linear. This is so because the combined load condition (1:0:1) stresses the plies primarily along the fiber direction as will be discussed in the theoretical study portion of the report. Combined-load stress-strain curves for axial compression with torsion (-1:0:-1) are shown in figure 11, and for transverse tension with torsion (0:1:-1) are shown in figure 12. Note that all the stress-strain curves in figure 11 and 12 are linear for the same reason given in discussing the curves in figure 10.

Combined load stress-strain curves for axial compression, transverse tension, and torsion (-1:1:-1) are shown in figure 13. Note that the axial stress, figure 13(a), and hoop stress, figure 13(b), stress-strain curves are slightly nonlinear for the same reasons mentioned in discussing the curves in figure 9. As can be observed, the other curves, figures 13(c) to (f), are linear.

Combined-load stress-strain curves for internal pressure (1:2:0) are shown in figure 14. As can be observed the curves are linear.

The results for all three gages for the axial compression load only (-1:0:0) are presented in figure 15. Note the different gage positions are identified 1, 2, and 3. As can be seen in figure 15(a) there is a small variation between the different gages. Possible reasons for the variation between rosettes are small load eccentricities, small ply misorientations, or rosette misalignment. The variation in the results of the rosettes shown in figure 15(b) are negligible. The shape of the shear strain curves, figure 15(c), is due to electronic noise in the system that appeared to be greatly magnified when attempts were made to measure very small (and perhaps insignificant) strains.

The important observations from the stress-strain curves are:

1. The Poisson's strain curve was linear for all the combined-loading conditions tested.

2. The stress-strain curves were nonlinear for cases with loading conditions (-1:1:0) or (-1:1:-1).

3. Small shear strains with normal loads indicate the presence of some type of coupling.

Combined-load stress-strain relationships. - The combined-load stress-strain relationships (also combined stress elastic coefficients or combined-load apparent stiffness) are summarized in Table III. Note in this table that three values of the combined-load stress-strain relationships are given. These are initial, intermediate, and final, and are so noted in the first column. The nominal stress ratio is given in the next three columns. The actual stresses are given in the mid-three columns headed by "Stress." The combined-load stress-strain

relationships are given in the columns headed by "Combined stress elastic coefficients," (last five columns in Table III). The numerical values in these five columns are tangents to the corresponding stress-strain curves at the initial, intermediate, and final points as determined by the computer program in reference 2.

As can be observed from the data in Table III, the initial, intermediate, and final values are in general not the same. This indicates some degree of nonlinearity for all the load combinations tested. This difference was not evident in the combined stress-strain curves discussed previously because of the smoothing effect in drawing the curves. Note the appreciable shear strains ($\epsilon_{cxy}/\epsilon_{cxx}$) (last column in Table III) for the uniaxial and combined-load cases without shear stress. Possible causes for these strains have been mentioned previously. The numerical data in Table III will be compared with predicted values in the comparisons section.

The important conclusion from the results and discussion of the experimental program is that one specimen, judiciously used, is sufficient to generate stress-strain relationships for many combined-load conditions. It is noted that this was the primary objective of this investigation.

THEORETICAL PROGRAM

The theoretical portion of this investigation consisted of using laminate theory (ref. 3) to investigate the following: combined-load elastic properties, combined-load effects on unbalanced laminates, laminate elastic properties sensitivity to ply shear modulus, combined-load ply stresses with and without residual stress, laminate fracture

stresses, and prediction of laminate fracture load. These are discussed sequentially in the following sections. The results obtained are subsequently compared with measured data.

Laminate Combined-Load Elastic Properties

The laminate combined-load elastic properties of interest in this investigation as previously defined are given by the following ratios:

apparent axial stiffness coefficient $\sigma_{cxx}/\epsilon_{cxx}$ (1)

apparent hoop stiffness coefficient $\sigma_{cyy}/\epsilon_{cyy}$ (2)

apparent shear stiffness coefficient $\sigma_{cxy}/\epsilon_{cxy}$ (3)

apparent axial-hoop coupling coefficient $\epsilon_{cyy}/\epsilon_{cxx}$ (4)

apparent axial-shear coupling coefficient $\epsilon_{cxy}/\epsilon_{cxx}$ (5)

The notation in the above ratios has been defined previously and is repeated here for convenience: σ denotes laminate stress; ϵ denotes laminate strain; the subscript c denotes laminate (composite) property; x and y denote laminate load axis (structural axes), figure 1. Note that the laminate apparent stiffnesses defined in the ratios (1) through (5) are similar to the stiffnesses defined under uniaxial loading. Note also that the apparent hoop-shear coupling stiffness may be readily obtained by dividing ratio (5) by ratio (4).

The laminate theory equations from which the various apparent stiffnesses in ratios (1) through (5) can be determined are given in matrix form by:

$$\begin{Bmatrix} \epsilon_{cxx} \\ \epsilon_{cyy} \\ \epsilon_{cxy} \end{Bmatrix} = \begin{bmatrix} 1/E_{cxx} & -\nu_{cyx}/E_{cyy} & \nu_{csx}/G_{cxy} \\ -\nu_{cxy}/E_{cxx} & 1/E_{cyy} & \nu_{csy}/G_{cxy} \\ \nu_{cxs}/E_{cxx} & \nu_{cys}/E_{cyy} & 1/G_{cxy} \end{bmatrix} \begin{Bmatrix} \sigma_{cxx} \\ \sigma_{cyy} \\ \sigma_{cxy} \end{Bmatrix} \quad (6)$$

The undefined notation in equation (6) is as follows: E denotes normal modulus; G, shear modulus; and ν, Poisson's ratio. The subscripts have the same meaning as noted previously.

For any combination of applied stress σ_{cxx}, σ_{cyy}, and σ_{cxy} the corresponding strains can be determined from equation (6). Knowing the stresses and the strains, the various apparent stiffness ratios in equations (1) through (5) are then determined.

The two important points to be observed from equation (6) are:

1. The presence of shear stress (σ_{cxy}) contributes to the laminate's normal stiffness and conversely through the coefficients ν_{csx}, etc.

2. The sense of the stress contributes to the laminate's stiffness. For example, shear stress σ_{cxy} with opposite sign to normal stress (σ_{cxx}) will reduce the axial strain ϵ_{cxx} and thus results in an apparent greater axial stiffness material as predicted by ratio (1).

Combined Stress Effects on Unbalanced Laminates

A balanced laminate is defined as that laminate which has an equal number of plies, identical in all respects, oriented at (+) and (-) orientation angles but necessarily symmetric with respect to bending. If this condition is not met, then the laminate is defined as unbalanced. Unbalanced laminates undergo shear when subjected to normal loads, that is, there is coupling between normal and shear deformations or stresses.

The coupling between normal and shear deformations is described mathematically by the coefficients ν_{csx}, ν_{csy}, ν_{cxs}, and ν_{cys} in equation (6). In a balanced laminate these coefficients are "zero." The coefficients (ν_{csx}), etc. are determined from ply properties and

orientation angle using laminate theory. Therefore, the combined stress effects on the stiffness of unbalanced laminates can be investigated theoretically. In the present investigation this was done by introducing small angle perturbations in the ply orientation angles of the laminate of interest and computing the coefficients ν_{cxs}, etc., using the computer code of reference 3. The results obtained are described later in the section entitled "COMPARISON OF MEASURED AND THEORETICAL DATA."

The importance of the previous discussion is that it leads to the following observation:

> When laminates believed to be balanced exhibit coupling between normal and shear deformations, then these laminates must have some plies misoriented. The degree of ply misorientation may be investigated theoretically using laminate theory.

Laminate Elastic Behavior Sensitivity

Some of the elastic properties of (±45) laminates are sensitive to ply misorientations and to ply shear modulus. Because of this sensitivity, incorrect values for ply orientation angles and/or ply shear modulus will produce disparities when comparing theoretical and measured results. In this section the sensitivity of laminate elastic properties to ply misorientations and to ply shear modulus are examined.

The sensitivity of the laminate elastic properties due to uniform misorientations in all plies is shown in figure 16. In this figure the variation of laminate (thin-tube) elastic properties [shear modulus (G_{cxy}), axial modulus (E_{cxx}), hoop modulus (E_{cyy}), and Poisson's

ratio (ν_{cxy})] is plotted as a function of decreasing ply perturbation angle about the 45^{o} direction. The corresponding sensitivity (variation) for increasing perturbation angles can be determined from figure 16 by noting the following:

1. G_{cxy} is symmetric about $\Delta\theta = 0$; that is 45^{o} ply angle.
2. Interchange E_{cxx} and E_{cyy}.
3. Compute ν_{cxy} from

$$\nu_{cxy(\Delta\theta>0)} = \left(\frac{E_{cyy}}{E_{cxx}}\nu_{cxy}\right)(\Delta\theta<0).$$

The interesting point to be observed from the curves in figure 16 is that:

The axial modulus (E_{cxx}), hoop modulus (E_{cyy}), and Poisson's ratio (ν_{cxy}) are sensitive to small ply perturbations (misorientations) about 45^{o} while the shear modulus is only slightly so. For example, a 2^{o} ply angle perturbation will produce about a 10 percent change in the axial and hoop moduli and Poisson's ratio. The corresponding change in the shear modulus will be about 0.5 percent.

The sensitivity of the laminate elastic properties due to variations in the ply shear modulus for a $\pm 45^{o}$ composite is shown in figure 17. In this figure the variation of the laminate (thin tube) elastic properties, shear modulus, axial or hoop modulus and Poisson's ratio is plotted as a function of ply shear modulus. As can be observed from figure 17, the laminate axial and hoop moduli and the Poisson's ratio are sensitive to and vary linearly with the ply shear modulus, while the laminate shear modulus is not sensitive. For example, a 10 percent variation in the

ply shear modulus at 1.0×10^6 psi will produce about 20 percent change in the laminate axial/hoop modulus and about 2.5 percent change in the laminate Poisson's ratio. The corresponding change in the shear modulus is identically zero.

The previous discussion leads to the following observation:

The in situ ply shear modulus will probably be needed to correlate predicted and theoretical data of elastic properties of angleplied laminates close to the $(\pm45)_s$ laminate configuration.

The in situ ply shear modulus may be determined indirectly from the sensitivity analysis described previously and the measured data. The observation that the in situ ply shear modulus may differ from that of the unidirectional composite has not been reported previously to the authors' knowledge.

Combined-Load Ply Stresses

The stresses in the plies of an angleplied laminate subjected to combined-load are computed using laminate theory, in general (ref. 3). When only one laminate configuration is considered, as is the case in the present investigation, it is convenient to compute the combined load ply stresses using ply-stress/composite-stress influence coefficients. These influence coefficients are generated by applying unit laminate stress σ_{cxx}, σ_{cyy}, or σ_{cxy} (fig. 1) and computing the resulting ply stresses along the fiber ($\sigma_{\ell 11}$), transverse to the fiber ($\sigma_{\ell 22}$) and intralaminar shear ($\sigma_{\ell 12}$) using laminate theory.

Once the ply-stress/composite-stress influence coefficients are available they can be used conveniently to make the following computation:

1. Computing ply stresses due to any combined-load laminate stress field (σ_{cxx}, σ_{cyy}, σ_{cxy}).
2. Estimating laminate fracture loads from ply failure stress limiting conditions.

For the $[\pm 45]_s$ laminate considered herein, the influence coefficients have been generated and are tabulated in matrix form in Table IV. Note in this table the ply stresses are given in the left-hand column, the composite (laminate) stresses in the right-hand column. There are two matrices of influence coefficients in Table IV. The first one is for the $+45^o$ ply and the second for the -45^o ply. The lamination residual stresses in the plies are given in Table V. These ply residual stresses were obtained via the laminate analysis of reference 3 by taking the difference between cure and room temperatures (-300^o F). The total ply stresses are obtained by computing the combined load stresses using the influence coefficients and then adding the ply residual stresses.

The important points to be observed from the influence coefficients and residual stress values for the $[\pm 45]_s$ laminate in Tables IV and V are:

1. Composite shear stress produces a ply longitudinal stress of about twice its magnitude and a ply transverse stress about 1/7 its magnitude.
2. Composite shear stress does not produce ply intralaminar shear stress.
3. Composite axial or hoop stress produces ply stresses of the following ply-stress to composite-stress relative magnitudes:

longitudinal	90 percent
transverse	10 percent
intralaminar shear	50 percent

4. The ply longitudinal residual stress is compressive, the transverse is tensile, and the intralaminar shear is zero. Note that the ply transverse residual stress exceeds the ply transverse strength, Table I. This means that some transply cracks could be present.

Laminate Failure Stresses and Loads

The failure stresses and loads at which the thin tube would fail were determined for the various combined-loading cases to which the tube was subjected. These failure stresses (loads) were obtained using the computer code of reference 3. They can also be readily determined by using the influence coefficients in Table IV in conjunction with the combined-stress failure criterion of reference 4.

The results obtained for failure stresses are summarized in Table VI. Note in this table the nominal combined-loading condition is given in the first three columns. Note also that lower and upper bounds are given on both laminate stress and strains. The lower bounds represent that laminate stress which is required to fail either the $+45^{\circ}$ or -45° ply (whichever occurs first in the given combined-loading condition). The upper bounds represent that stress state which is required to fail the unfailed ply as well. In determining these bounds the residual stresses were neglected because:

1. The lamination residual stress was sufficiently high (Table V) to fail the ply in transverse tension as was previously noted.

2. The various combined-loadings in the laminate are resisted by ply longitudinal and intralaminar shear stresses as can be observed from the influence coefficients in Table IV.

The laminate failure stresses are readily converted to corresponding loads using the tube geometry and can be compared to the experimental results.

The important point to be observed from the results in Table VI is the following:

For the majority of the combined loading-condition cases the two bounds are about the same. The exceptions are:

(1) the uniaxial shear case (0:0:1)

(2) the combined load case (1.5:1:1).

It is noted in passing that loading conditions producing approximately equal lower and upper bounds result in efficient material utilization. Those producing wide bounds can be used to meet fail-safe design requirements.

COMPARISON OF MEASURED AND THEORETICAL DATA

The comparisons of the measured and theoretical data consist of comparing results for the apparent stiffness and for the fracture load. These comparisons are described and discussed below.

Comparison of Apparent Stiffnesses

The apparent stiffness results were compared as follows:

1. Theoretical results with measured data from manually drawn initial tangent to the stress-strain curve.
2. Theoretical results with measured data from curve-fitted initial tangent.
3. Theoretical results with measured data from curve-fitted tangent at intermediate strain.

Comparison results with the manually-drawn initial tangent to the stress-strain curve are summarized in Table VII. Note in Table VII the nominal combined-loading condition is given in the first three columns. The apparent stiffnesses ($\sigma_{cxx}/\epsilon_{cxx}$, etc.) are given by their corresponding symbols defined previously and also in the table for convenience. The measured properties are listed under columns headed by "M" and the theoretical predictions under "P." As can be observed, the comparisons for the various stiffnesses are in good agreement. Though no percentage values are given in the table, the comparisons of the majority of the cases are within 10 percent. A few exceptions are for combined-loading cases of normal with shear such as (1:0:1). The discrepancies here are believed to be caused by small errors in ply angle orientations which result in coupling between normal and shear displacements. Numerical experiments to support this belief showed that if the two -45^{o} plies were oriented at -44^{o} and -43^{o}, respectively, the predicted apparent stiffness $\sigma_{cxy}/\epsilon_{cxy}$ decreased from 7.7×10^{6} to 7.3×10^{6} psi (6.8×10^{6} psi measured) and $\epsilon_{cyy}/\epsilon_{cxx}$ decreased from -0.69 to -0.78 (-0.77 measured).

Comparison results with the curve-fitted initial tangent data are summarized in Table VIII. As can be observed, the comparisons are about the same as for the previous table.

Comparison results with curve-fitted tangent at intermediate strain are summarized in Table IX. As can be observed from the results in this table, the comments already made in connection with the results in the preceding two tables apply to Table IX as well.

The preceding discussion leads to the following observations:

1. The plies in a thin angleplied laminated tube undergo nonlinear shear deformation (1.54×10^6 psi ply shear modulus for predicting initial tangent properties and 1.22×10^6 psi for 50 percent strain properties).

2. The combined-stress apparent stiffnesses are quite sensitive to small ply misorientations (1° or 2° when the nominal ply angle is $\pm 45^\circ$).

3. The laminate theory predicts laminate apparent stiffnesses which are in good agreement with measured data provided that corrected values for the in situ ply shear modulus and ply orientation angles are used.

Comparison of Fracture Stresses

The specimen was loaded to fracture in the combined loading-condition (1:0:1.2). The predicted and measured laminate stresses at fracture for this case are as follows (refer to Tables II, VI):

Stress type	Stress value (ksi)		
	Measured	Predicted	
		Lower bound	Upper bound
Axial	20.2	17.9	19.4
Torsional	23.1	20.6	22.3

As can be seen, the measured fracture stresses are about 4 percent higher than the predicted upper bound. This is considered to be very good agreement.

An important conclusion from the previous discussion is that the in situ ply properties may be required to predict angleplied laminate fracture using linear laminate theory.

GENERAL COMMENTS

From the results and discussion of the present investigation the following general comments can be made regarding the use of composites for structural components. In the case of thin composite tubes suitable for torque transmission shafts the laminate configuration should be $[\pm 45]_s$, other design requirements permitting. Recall that in this laminate configuration the torque is resisted only by longitudinal stress in the plies, and therefore, the ply transverse residual stresses present are not magnified by the application of torque.

In designs where thermal distortion minimization is a requirement, a $[\pm 45]_s$ laminate configuration may be a good choice. Composites which provide good thermal distortion stability (such as graphite/resin) will more than likely exhibit transply cracks due to lamination residual stress. Recall that the transverse ply stresses in the $[\pm 45]_s$ laminate loaded axially are about 10 percent of the corresponding longitudinal stresses. Therefore, only minimal stresses will be resisted by the already weakened transverse ply direction.

In designs where resistance to impact is a criterion, the component should be sized so that the anticipated combined-loading does not produce biaxial stress ratios resulting in high apparent stiffness. The reason for this is that high apparent stiffness is associated with low-strain-to-fracture, Table III.

SUMMARY OF RESULTS

The significant results of the investigation to measure and predict the combined-load apparent stiffnesses of angleplied laminates using a

single thin tube and subjecting it to a number of combined-loading conditions are as follows:

1. One thin composite tube, properly instrumented and with a priori estimates on its fracture stresses, can be used to measure the combined-stress apparent stiffness of angleplied laminates subjected to a large number of different combined-loading conditions.

2. Laminate theory can predict results which are in good agreement with measured data for both apparent stiffness and fracture stress provided that the in situ ply properties are reasonably well represented.

3. The laminate apparent and actual stiffnesses are sensitive to ply shear modulus and to ply misorientations when the angleplied-laminate nominally consists of $\pm 45^{\circ}$ plies.

4. The laminate apparent stiffness is sensitive to both combined-loading stress magnitude and sense.

5. Unbalanced angleplied laminates, resulting from small ply misorientations exhibit lower apparent shear stiffness than their balanced counterparts when subjected to combined normal and shear loadings.

6. The plies in a $[\pm 45_2]_s$ angleplied laminate subjected to combined-loadings undergo nonlinear shear deformations even at low strain relative to uniaxial fracture strain.

7. The in situ ply shear modulus in thin tube angleplied laminates appears to be different (50 percent higher) than that measured in a unidirectional composite.

REFERENCES

1. Bert, C. W., "Experimental Characterization of Composites," Structural Design and Analysis, Part II, vol. 8, C. C. Chamis, ed., Academic Press, 1975, p. 73.

2. Chamis, C. C., Kring, J. F., and Sullivan, T. L., "Automated Testing Data Reduction Computer Program," ASTM Conference on Analysis of Test Methods for High Modulus Fibers and Composites, San Antonio, Texas, April 1972.

3. Chamis, C. C., "Computer Code for the Analysis of Multilayered Fiber Composites-Users Manual," NASA Lewis Research Center, Cleveland, Ohio, TN D-7013.

4. Chamis, C. C., "Failure Criteria for Filamentary Composites," NASA Lewis Research Center, Cleveland, Ohio, TN D-5367.

TABLE I. - BORON/EPOXY UNIDIRECTIONAL COMPOSITE[a] NOMINAL PROPERTIES AT ROOM TEMPERATURE

Property	Units	
Fiber diameter	in.	0.004
Fiber volume ratio	------	.50
Composite density	$lb/in.^3$	.07
Ply thickness	in.	.005
Longitudinal thermal coefficient of expansion	10^{-6} in./in./°F	2.4
Transverse thermal coefficient of expansion	10^{-6} in./in./°F	16.7
Longitudinal modulus	10^6 psi	29.5
Transverse modulus	10^6 psi	2.8
Shear modulus	10^6 psi	.8
Major Poisson's ratio	------	.24
Longitudinal tensile strength	ksi	204
Longitudinal compressive strength	ksi	240
Transverse tensile strength	ksi	9
Transverse compressive strength	ksi	40
Intralaminar shear strength	ksi	10

[a]Contains glass scrim.

TABLE II. - SUMMARY OF STRESS COMBINATIONS FOR A $[(\pm 45)_2]_s$ BORON/EPOXY THIN TUBE SPECIMEN FOR VARIOUS LOADING CONDITIONS

Nominal loading condition			Final average composite stress, psi			
Axial	Hoop	Torsional	Axial	Hoop	Torsional	Comments
1	0	0	4700	0	0	
-1	0	0	-4660	0	0	
0	1	0	0	4930	0	
0	0	1	0	0	7670	
0	0	-1	0	0	-7640	
1	1	0	4830	4930	0	
-1	1	0	-4580	4600	0	
1	0	1	1840	0	1800	
-1	0	-1	-1830	0	-1740	
0	1	-1	-----	4610	-5050	
-1	1	-1.5	-2310	2320	-3310	
1	2	0	2450	5000	0	
1	0	1.2	20190	0	23150	Fracture

TABLE III. - SUMMARY OF MEASURED COMBINED STRESS ELASTIC COEFFICIENTS FOR A BORON/EPOXY $\left[(\pm 45)_2\right]_s$ COMPOSITE TUBE, AT 0.5 FIBER VOLUME RATIO AND ZERO VOIDS

Load condition							Combined stress elastic coefficients, 10^6 psi					Load condition							Combined stress elastic coefficients, 10^6 psi				
Designation				Stress, psi								Designation				Stress, psi							
At	Type			Axial A	Hoop H	Torque T	σ_{cxx} / ϵ_{cxx}	σ_{cyy} / ϵ_{cyy}	σ_{cxy} / ϵ_{cxy}	ϵ_{cyy} / ϵ_{cxx}	ϵ_{cxy} / ϵ_{cxx}	At	Type			Axial A	Hoop H	Torque T	σ_{cxx} / ϵ_{cxx}	σ_{cyy} / ϵ_{cyy}	σ_{cxy} / ϵ_{cxy}	ϵ_{cyy} / ϵ_{cxx}	ϵ_{cxy} / ϵ_{cxx}
	A	H	T										A	H	T								
Initial	1	0	0	0	0	0	6.3	0	0	-0.72	-0.04	Initial	-1	1	0	0	0	0	3.2	2.7	0	-1.1	-0.21
Interm.				3100	0	0	4.8	0	0	-.81	-.05	Interm.				-2900	2900	0	1.8	1.7	0	-1.1	-.07
Final				4700	0	0	4.0	0	0	-.71	-.12	Final				-4600	4600	0	1.3	1.3	0	-.91	-.07
Initial	-1	0	0	0	0	0	4.8	0	0	-.78	-.16	Initial	1	0	1	0	0	0	4.7	0	5.7	-.84	.87
Interm.				-2700	0	0	4.5	0	0	-.80	-.06	Interm.				1100	0	1100	4.5	0	6.1	-.83	.71
Final				-4700	0	0	4.1	0	0	-.91	-.07	Final				1800	0	1800	4.6	0	6.3	-.74	.82
Initial	0	1	0	0	0	0	0	4.1	0	-1.6	.13	Initial	0	1	-1	0	0	0	0	4.7	5.3	-1.5	1.3
Interm.				0	3100	0	0	3.6	0	-1.4	.03	Interm.				0	2900	-3100	0	3.4	6.2	-1.4	.86
Final				0	4900	0	0	3.2	0	-----	-.01	Final				0	4600	-5100	0	2.8	5.6	-5.0	2.4
Initial	0	0	1	0	0	0	0	0	7.4	0	0	Initial	-1	0	-1	0	0	0	4.64	0	5.9	-.74	.70
Interm.				0	0	4800	0	0	8.2	0	0	Interm.				-1100	0	-1100	4.34	0	7.6	-.68	.50
Final				0	0	7600	0	0	8.3	0	0	Final				-1800	0	-1700	5.5	0	4.7	-.74	.90
Initial	0	0	1	0	0	0	0	0	7.7	0	0	Initial	1.5	1	1	0	0	0	7.8	5.4	5.6	-.06	-.73
Interm.				0	0	4800	0	0	7.8	0	0	Interm.				9050	5520	5870	8.8	6.0	6.7	-.14	-.92
Final				0	0	7700	0	0	7.7	0	0	Final				13400	9130	9950	8.3	5.7	6.3	-.24	-.90
Initial	1	1	0	0	0	0	25.0	12.0	0	1.7	-.24	Initial	-1	1	-1	0	0	0	2.7	2.5	5.4	-1.1	.70
Interm.				3000	3100	0	23.0	15.0	0	1.8	-.22	Interm.				1730	1740	2500	2.0	1.9	5.9	-1.1	.50
Final				4900	5000	0	12.0	11.0	0	.25	-.12	Final				2300	2300	3300	1.8	1.6	5.9	-1.0	.40
Initial	1	1	0	0	0	0	24.0	11.0	0	2.2	-.44	Initial	1	2	0	0	0	0	-2.0	3.0	0	-1.4	-.1
Interm.				3000	3000	0	19.0	15.0	0	1.3	-.8	Interm.				1500	3000	0	-10.0	7.0	0	-3.4	-.5
Final				4800	3900	0	----	----	0	---	-.24	Final				2500	5000	0	-8.8	6.9	0	-2.6	-.6

Notation: A, H, T denote axial, hoop, torsional, respectively.

TABLE IV. - INFLUENCE COEFFICIENTS FOR CALCULATING

PLY STRESSES FROM COMPOSITE STRESSES

$$\begin{Bmatrix} \sigma_{\ell 11} \\ \sigma_{\ell 22} \\ \sigma_{\ell 12} \end{Bmatrix} = \begin{bmatrix} a_{11} & a_{12} & a_{13} \\ a_{21} & a_{22} & a_{23} \\ a_{31} & a_{32} & a_{33} \end{bmatrix} \begin{Bmatrix} \sigma_{cxx} \\ \sigma_{cyy} \\ \sigma_{cxy} \end{Bmatrix}$$

(Ply stress) (Influence coefficients) (Composite stress)

$$\begin{bmatrix} 0.90 & 0.90 & 1.86 \\ .10 & .10 & -.14 \\ -.50 & .50 & 0 \end{bmatrix}$$

$+45^{\circ}$ Ply and no residual stress

$$\begin{bmatrix} 0.90 & 0.90 & -1.86 \\ .10 & .10 & .14 \\ .50 & -.50 & 0 \end{bmatrix}$$

-45° Ply and no residual stress

TABLE V. - RESIDUAL STRESS + OR -45° PLY

FOR A TEMPERATURE DIFFERENCE OF -300° F

$$\begin{Bmatrix} \sigma_{\ell 11} \\ \sigma_{\ell 22} \\ \sigma_{\ell 12} \end{Bmatrix} = \begin{Bmatrix} -10.5 \\ 10.5 \\ 0 \end{Bmatrix} \text{(ksi)}$$

TABLE VI. - PREDICTED LAMINATE FAILURE STRESS BOUNDS FOR $\left[\pm 45_2\right]_s$ BORON/EPOXY LAMINATE, 0.5 FIBER VOLUME RATIO, ZERO VOIDS AND NO RESIDUAL STRESS

Nominal loading condition			Lower bounds						Upper bounds					
			Stress (ksi)			Strain, 10^{-3} in./in.			Stress (ksi)			Strain, 10^{-3} in./in.		
A	H	T	A	H	T	A	H	T	A	H	T	A	H	T
1	0	0	20.0	0	0	4.7	-3.5	0	20.0	0	0	4.7	-3.5	0
-1	0	0	-20.6	0	0	-4.8	3.6	0	-20.6	0	0	-4.8	3.6	0
0	0	1	0	0	55.9	0	0	7.1	0	0	99.4	0	0	12.7
1	1	0	46.2	46.2	0	2.8	2.8	0	46.2	46.2	0	2.8	2.8	0
-1	1	0	-10.3	10.3	0	-4.2	4.2	0	-10.3	10.3	0	-4.2	4.2	0
1	0	1	18.0	0	18.0	4.3	-3.2	2.3	19.3	0	19.3	4.6	-3.2	2.5
-1	0	-1	-18.5	0	-18.5	-4.6	3.4	-2.3	-19.3	0	-19.3	-4.7	3.5	-2.4
0	1	-1	0	19.1	-19.1	-3.1	4.4	-2.6	0	20.6	-20.6	-3.4	4.7	-2.8
-1	1	-1.5	-9.9	9.9	-13.9	-3.9	3.9	-1.8	-10.1	10.1	-14.5	-4.1	4.1	-1.9
1	2	0	16.9	33.9	0	-2.0	5.0	2.6	16.9	33.9	0	-2.0	5.0	2.6
1	0	1.2	17.9	0	20.6	4.2	-3.1	2.7	19.4	0	22.3	4.6	-3.4	2.9
1.5	1	1	16.4	11.4	12.5	1.87	-.29	1.62	32.3	22.4	24.8	3.73	-.50	3.28

Notes: 1. Lower bounds are based on first ply failure.
2. Upper bounds are based on second ply failure.
3. A, H, T denote axial, hoop, torsional, respectively.

TABLE VII. - COMPARISON OF INITIAL TANGENT PREDICTED AND MEASURED COMBINED STRESS ELASTIC COEFFICIENTS FOR A BORON EPOXY $\left[(\pm 45)_2\right]_s$ COMPOSITE TUBE AT 0.5 FIBER VOLUME RATIO AND HAVING NO VOIDS

[Measured coefficients were determined from manually drawing initial tangent.]

Combined load			Combined stress elastic coefficients (apparent stiffness)									
Axial	Hoop	Torque	$\sigma_{cxx}/\epsilon_{cxx}$, 10^6 psi		$\sigma_{cyy}/\epsilon_{cyy}$, 10^6 psi		$\sigma_{cxy}/\epsilon_{cxy}$, 10^6 psi		$\epsilon_{cyy}/\epsilon_{cxx}$		$\epsilon_{cxy}/\epsilon_{cxx}$	
			M	P	M	P	M	P	M	P	M	P
1	0	0	5.8	5.2	0	0	0	0	-0.75	-0.69	0	0
-1	0	0	5.2	5.2	0	0	0	0	-.79	-.69	0	0
0	1	0	0	0	6.5	5.2	0	0	-1.5	-1.4	0	0
0	0	1	0	0	0	0	8.0	7.8	0		0	0
1	1	0		17.0		17.0		0	1.0	1.0		0
-1	1	0	3.0	3.1	2.6	3.1	0		-1.05	-1.0	0	0
1	0	1	4.9	5.2	0	0	6.8	7.8	-.77	-.69	0.69	0.67
-1	0	-1	4.7	5.2	0	0	6.6	7.8	-.75	-.69	.69	.67
0	1	-1	0	0	4.8	5.2	6.6	7.8	-1.4	-1.4	.64	.96

Notation: σ, ϵ denote stress, strain.
x, y denote direction with x-axial and y-hoop.
M, P denote measured, predicted.

TABLE VIII. - COMPARISON OF INITIAL TANGENT PREDICTED AND MEASURED COMBINED STRESS ELASTIC COEFFICIENTS FOR A BORON/EPOXY $\left[(\pm 45)_2\right]_s$ COMPOSITE TUBE AT 0.5 FIBER VOLUME RATIO AND HAVING NO VOIDS

[Measured properties as determined by the computed initial tangent of the curve-fitted data.]

Combined load			Combined stress elastic coefficients									
Axial	Hoop	Torque	$\sigma_{cxx}/\epsilon_{cxx}$, 10^6 psi		$\sigma_{cyy}/\epsilon_{cyy}$, 10^6 psi		$\sigma_{cxy}/\epsilon_{cxy}$, 10^6 psi		$\epsilon_{cyy}/\epsilon_{cxx}$		$\epsilon_{cxy}/\epsilon_{cxx}$	
			M	P	M	P	M	P	M	P	M	P
1	0	0	[a]5.2	5.2	0	0	0	0	[a]-0.72	-0.69	0	0
0	1	0	0	0	[a]5.2	5.2	0	0	-.65	-.69	0	0
0	0	1	0	0	0	0	7.6	7.8	0	0	0	0
1	1	0	[a]19.5	17.0	[a]19.5	17.0	0	0	[a]1.2	1.0	0	0
-1	1	0	3.2	3.1	2.7	3.1	0	0	-1.1	-1.0	0	0
1	0	1	4.7	5.2	0	0	5.7	7.8	-.84	-.69	-0.87	0.67
-1	0	-1	4.6	5.2	0	0	5.9	7.8	-.74	-.69	-.70	.67
0	1	-1	0	0	4.7	5.2	5.3	7.8	-.67	-1.4	.87	.96
1	1	1		17.0		17.0		7.8		1.0		2.2
-1	1	-1	2.7	3.1	2.5	3.1	5.4	7.8	-1.10	-1.0	-.7	.39
1	2	0	2.0	-14.0	3.0	8.0	0	7.8	-1.4	-3.4	0	0

[a]Averages of values from similar load cases on Table III.

Notation: σ, ϵ denote stress, strain.
x, y denote direction with x-axial and y-hoop.
M, P denote measured, predicted.

TABLE IX. - COMPARISON OF INTERMEDIATE STRAIN PREDICTED AND MEASURED COMBINED STRESS ELASTIC COEFFICIENTS FOR A BORON/EPOXY $\left[(\pm 45)_2\right]_s$ COMPOSITE TUBE AT 0.5 FIBER VOLUME RATIO

Combined load			Combined stress elastic coefficients									
Axial	Hoop	Torque	σ_{cxx} ϵ_{cxx},		$\sigma_{cyy}/\epsilon_{cyy}$,		$\sigma_{cxy}/\epsilon_{cxy}$,		$\epsilon_{cyy}/\epsilon_{cxx}$		$\epsilon_{cxy}/\epsilon_{cxx}$	
			10^6 psi		10^6 psi		10^6 psi		M	P	M	P
			M	P	M	P	M	P				
1	0	0	4.2	4.3	0	0	0	0	-0.76	-0.75	0	0
0	1	0	0	0	4.2	4.3	0	0	-1.3	-1.3	0	0
0	0	1	0	0	0	0	8.2	7.8	-----	-----	----	----
1	1	0	17.8	17.0	17.8	17.0	0	0	1.1	1.0	0	0
-1	1	0	1.8	2.5	1.7	2.5	0	0	-1.1	-1.0	0	0
1	0	1	4.5	4.3	0	0	6.1	7.8	-.83	-.75	0.71	0.55
-1	0	-1	4.3	4.3	0	0	7.6	7.8	-.68	.75	.50	.55
0	1	-1	0	0	3.4	4.3	6.3	7.8	-1.4	-1.3	.86	.74
1.5	1	1	8.8	8.8	5.9	4.6	6.9	7.8	-.14	-.13	.92	.84
-1	1	-1	2.0	2.5	2.0	2.5	5.9	7.8	-1.1	-1.0	.50	.32
1	2	0	-10.0	-8.7	7.0	6.9	0	0	-3.4	-2.5	0	0

Notation: σ, ϵ denote stress, strain.
x, y denote directions with x-axial and y-hoop.
M, P denote measured, predicted.

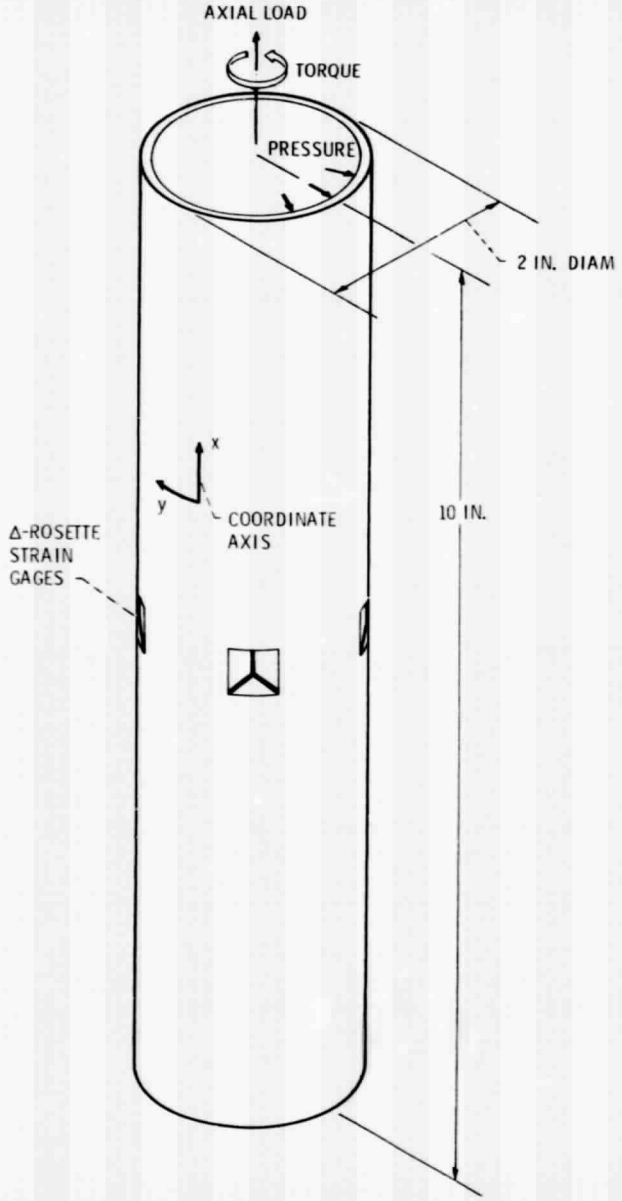

Figure 1. - Schematic of composite tube specimen showing loads and instrumentation.

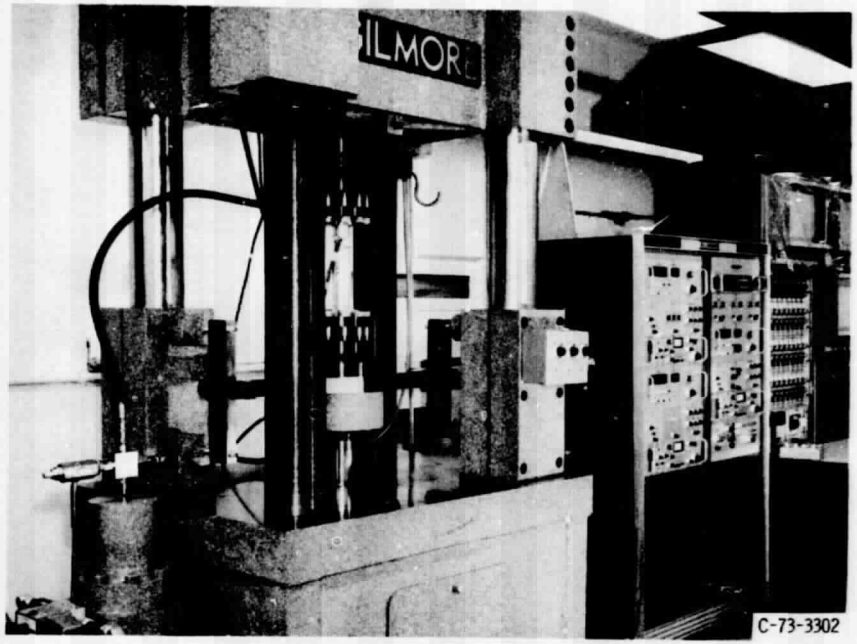

Figure 2. - Multiaxial testing facility for composite tubes.

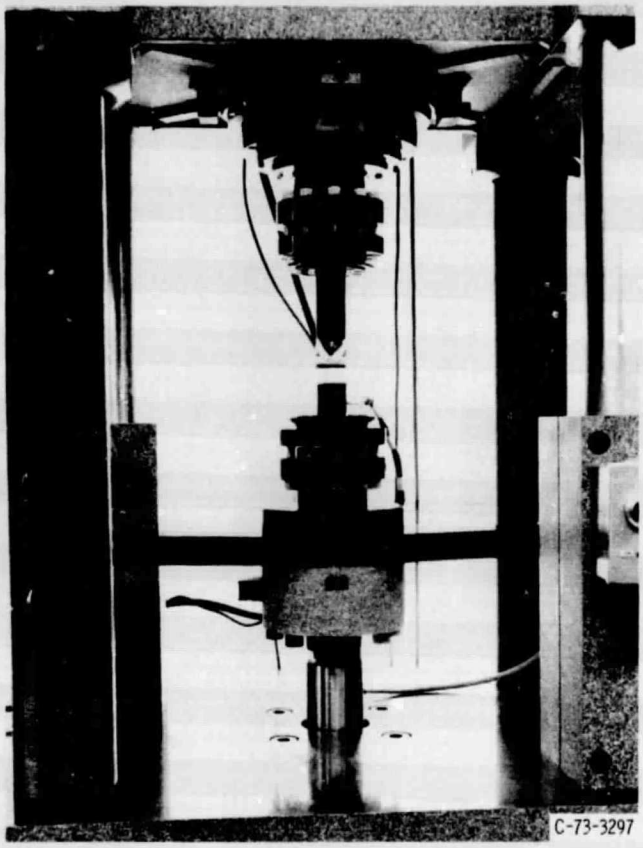

(a) IN TESTING MACHINE.

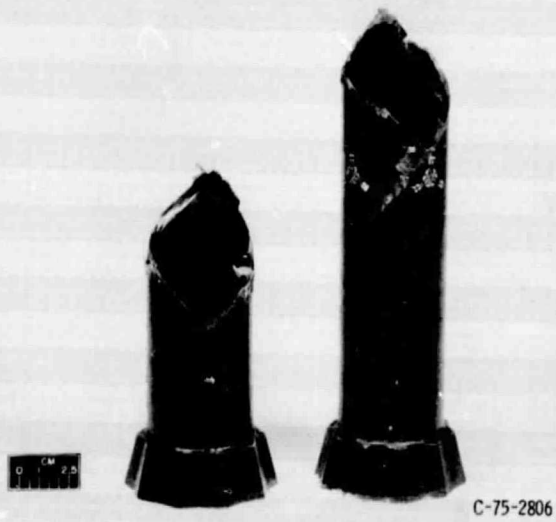

(b) AFTER FRACTURE.

Figure 3. - Instrumented Boron/Epoxy $[(\pm 45)_2]_s$ composite tube specimen.

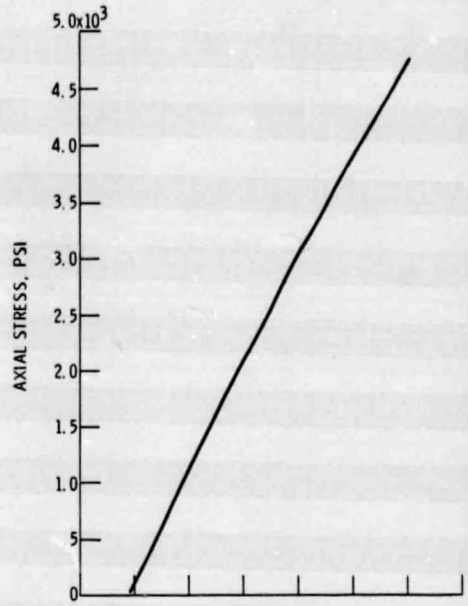

(a) AXIAL STRESS.

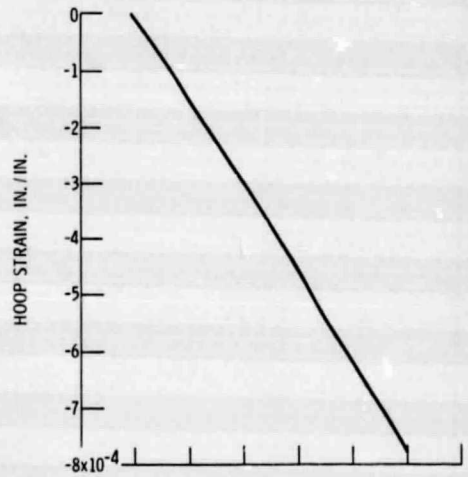

(b) HOOP STRAIN.

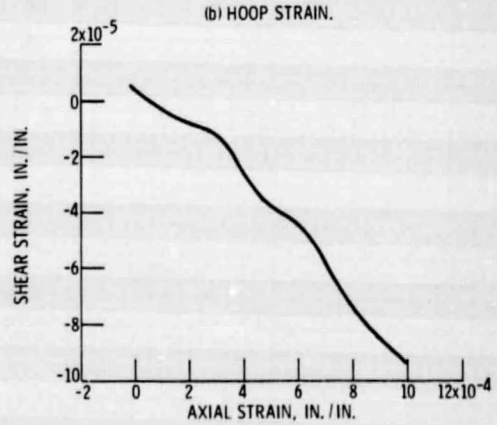

(c) SHEAR STRAIN.

Figure 4. - Stress-strain and strain-strain curves for a thin composite tube subjected to axial tension (1:0:0). $[\pm 45)_2]_s$ boron/epoxy, 0.50 fiber volume ratio.

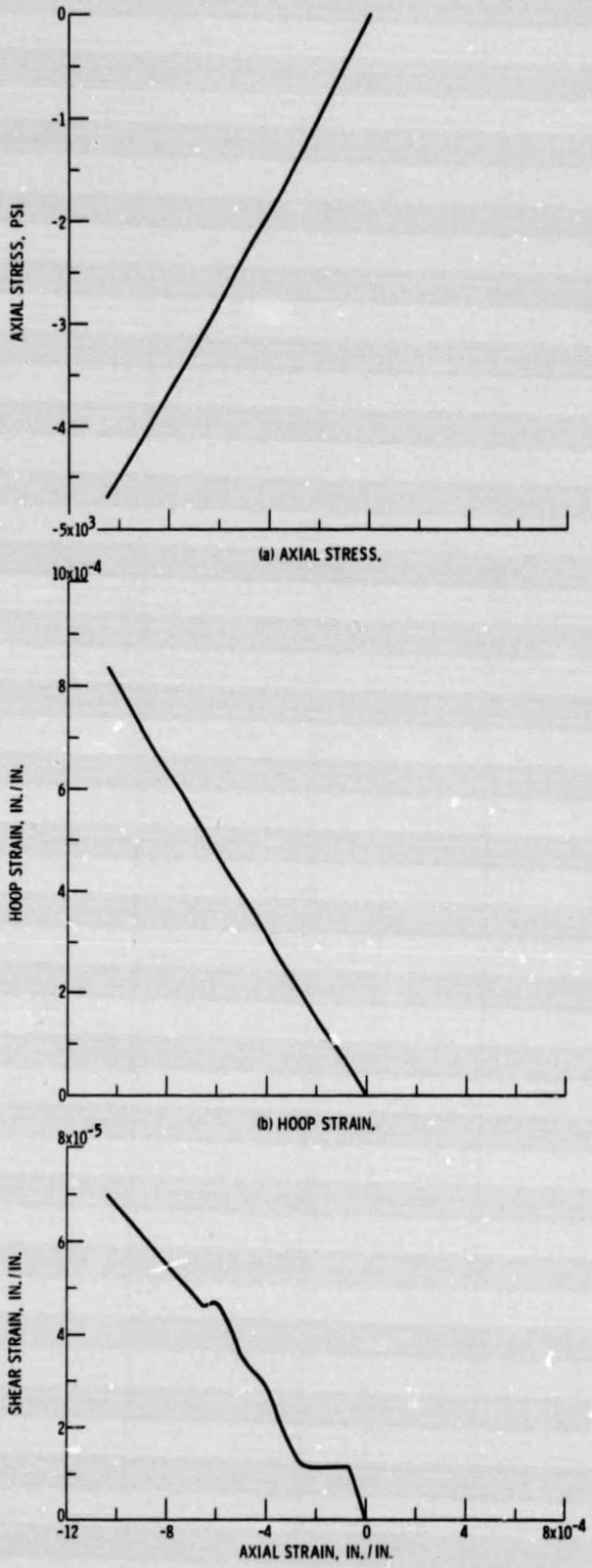

Figure 5. - Stress-strain and strain-strain curves for a thin composite tube subjected to axial compression (-1:0:0). $[\pm 45]_2]_s$ boron/epoxy, 0.50 fiber volume ratio.

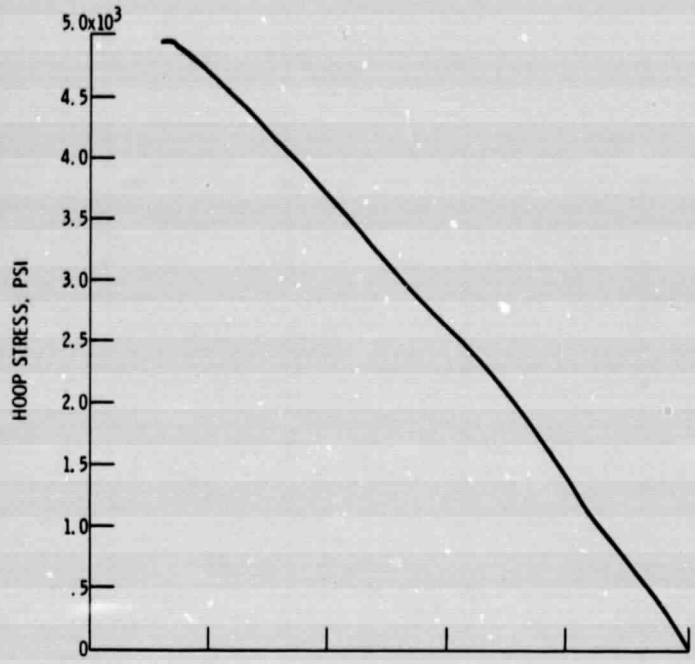

(a) HOOP STRESS.

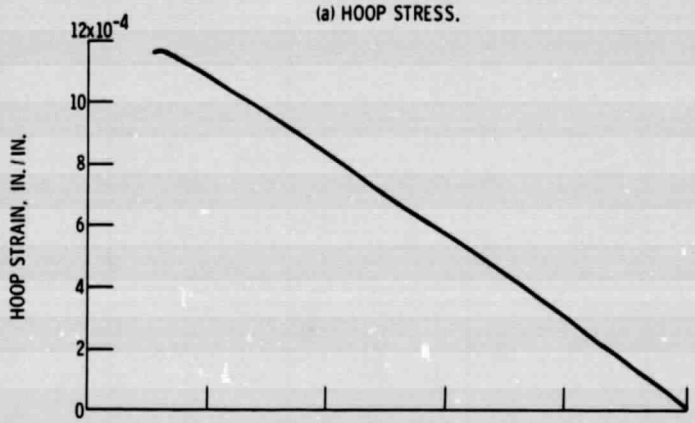

(b) AXIAL STRAIN.

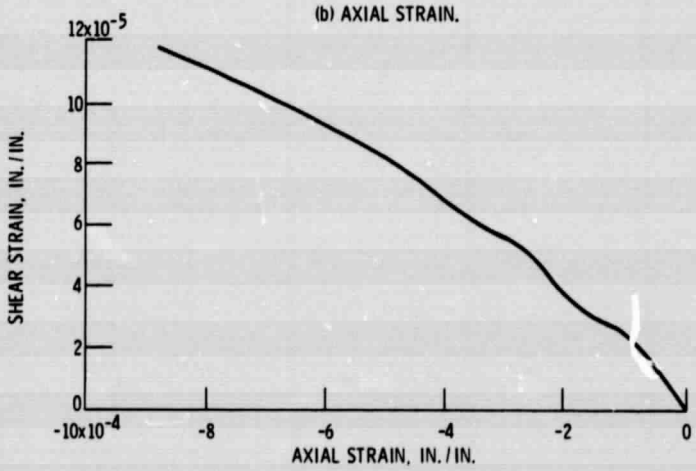

(c) SHEAR STRAIN.

Figure 6. - Stress-strain curves for a thin composite tube subjected to hoop tension (0:1:0). $[\pm 45_2]_s$ boron/epoxy, 0.50 fiber volume ratio.

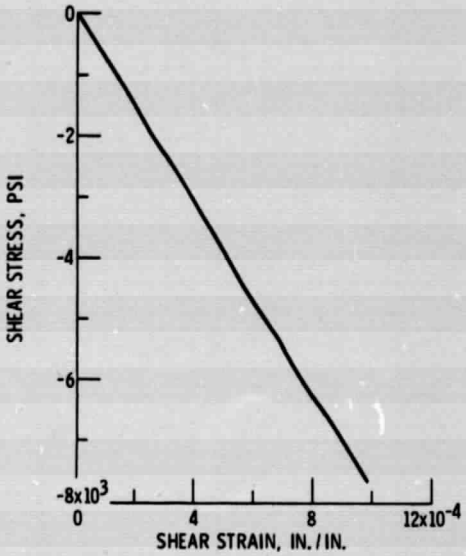

Figure 7. - Stress-strain curve for a thin composite tube subjected to torsion (0:0:1). $[(\pm 45)_2]_s$ boron/epoxy, 0.50 fiber volume ratio.

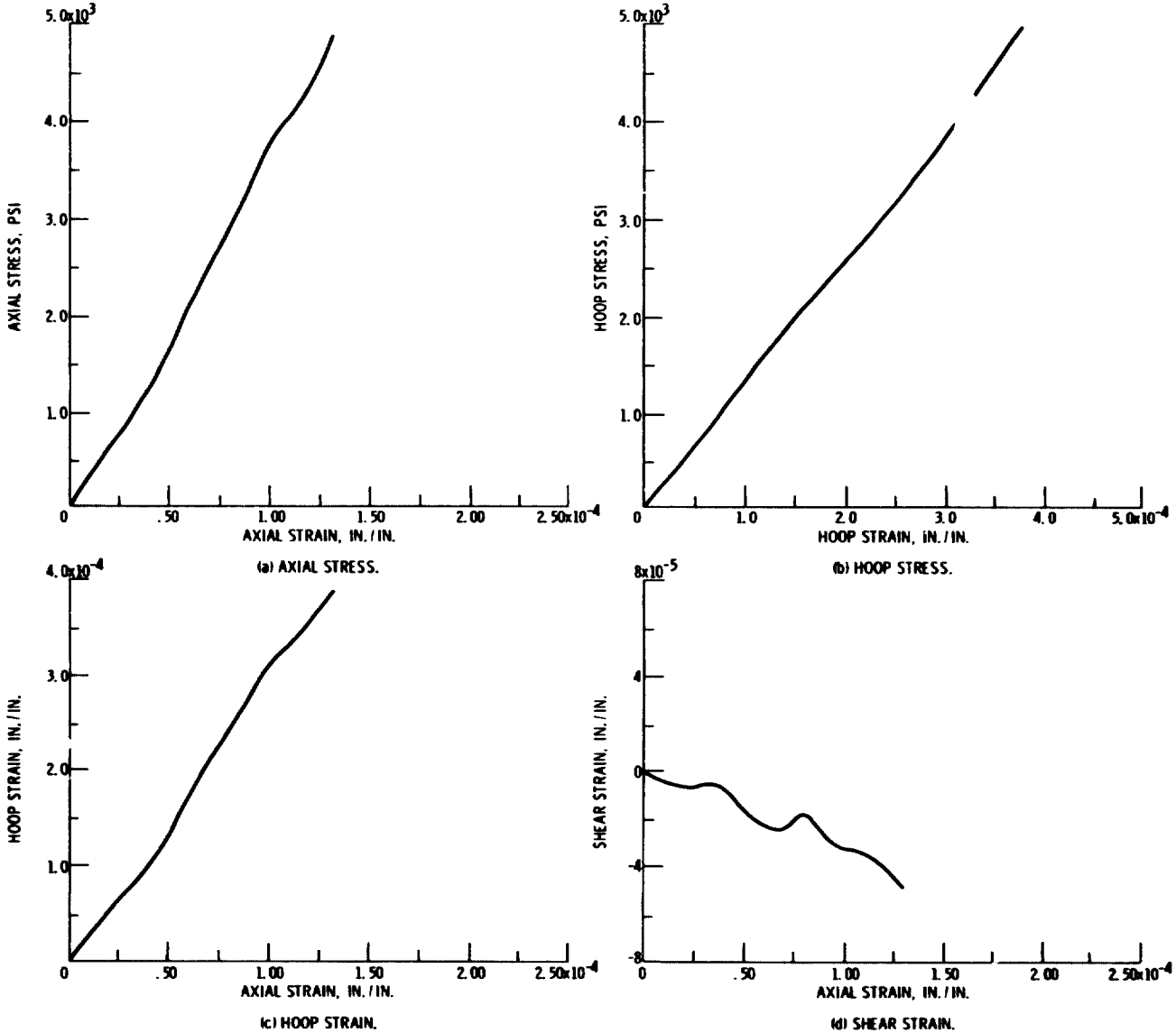

Figure 8. - Stress-strain and strain-strain curves for a thin composite tube subjected to combined load stress ratio (1:1:0). $[\pm 45]_2]_s$ boron/epoxy, 0.50 fiber volume ratio.

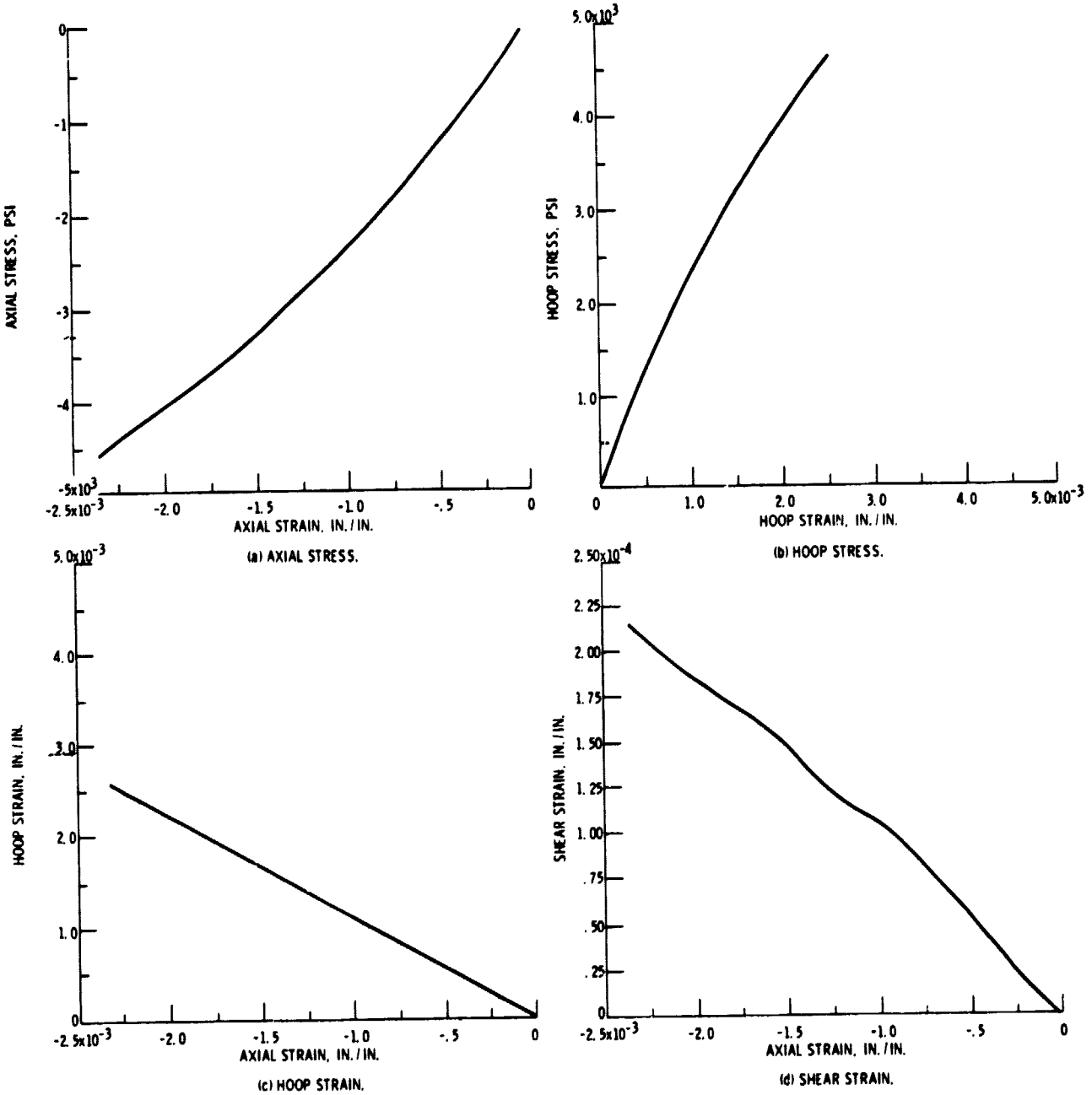

Figure 9. - Stress-strain and strain-strain curves for a thin composite tube subjected to combined load stress ratio (-1:1:0). $[(\pm 45)_2]_s$ boron/epoxy, 0.50 fiber volume ratio.

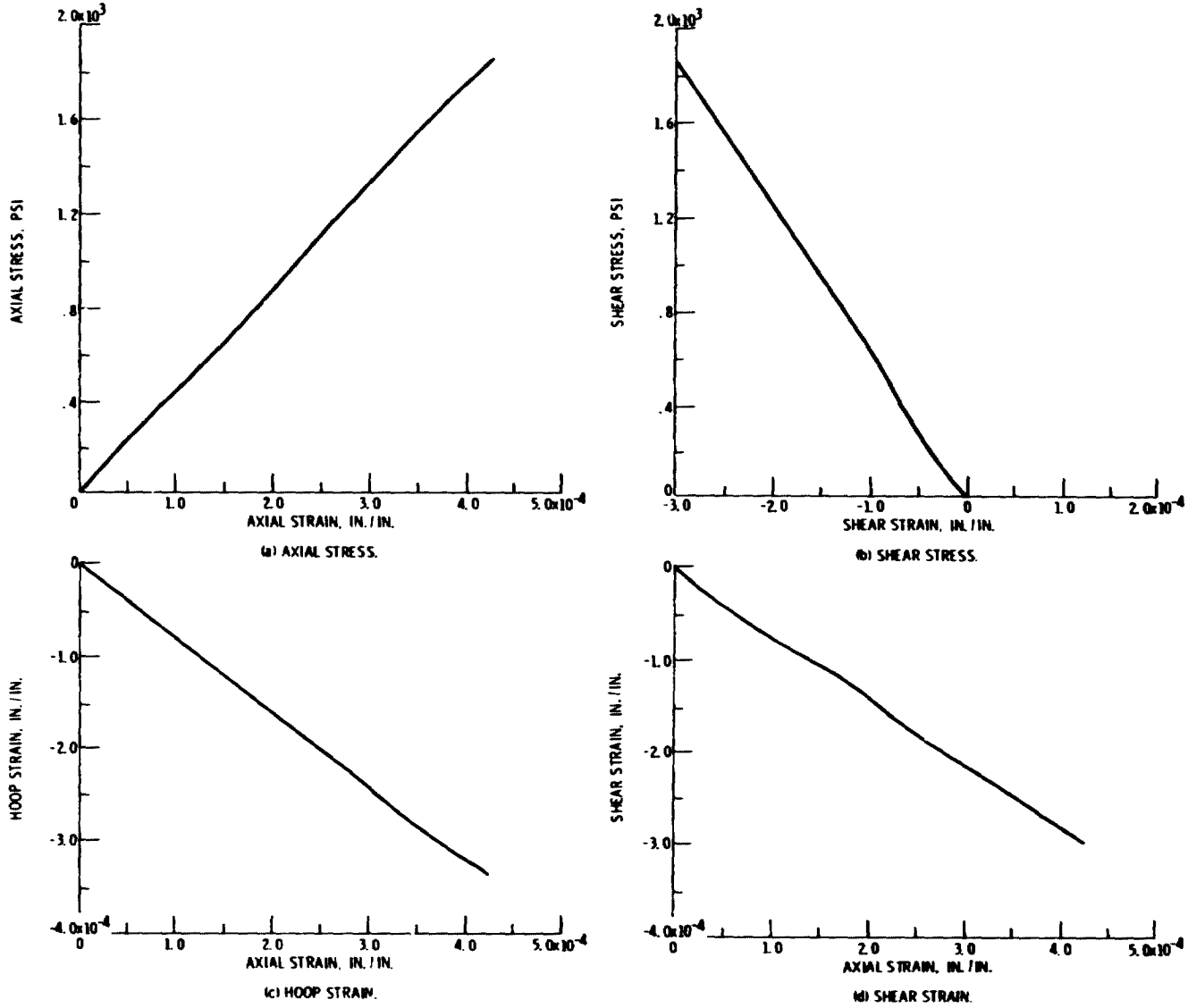

Figure 10. - Stress-strain and strain-strain curves for a thin composite tube subjected to combined load stress ratio (1:0:1). $[\pm 45]_{2_S}$ boron/epoxy. 0.50 fiber volume ratio.

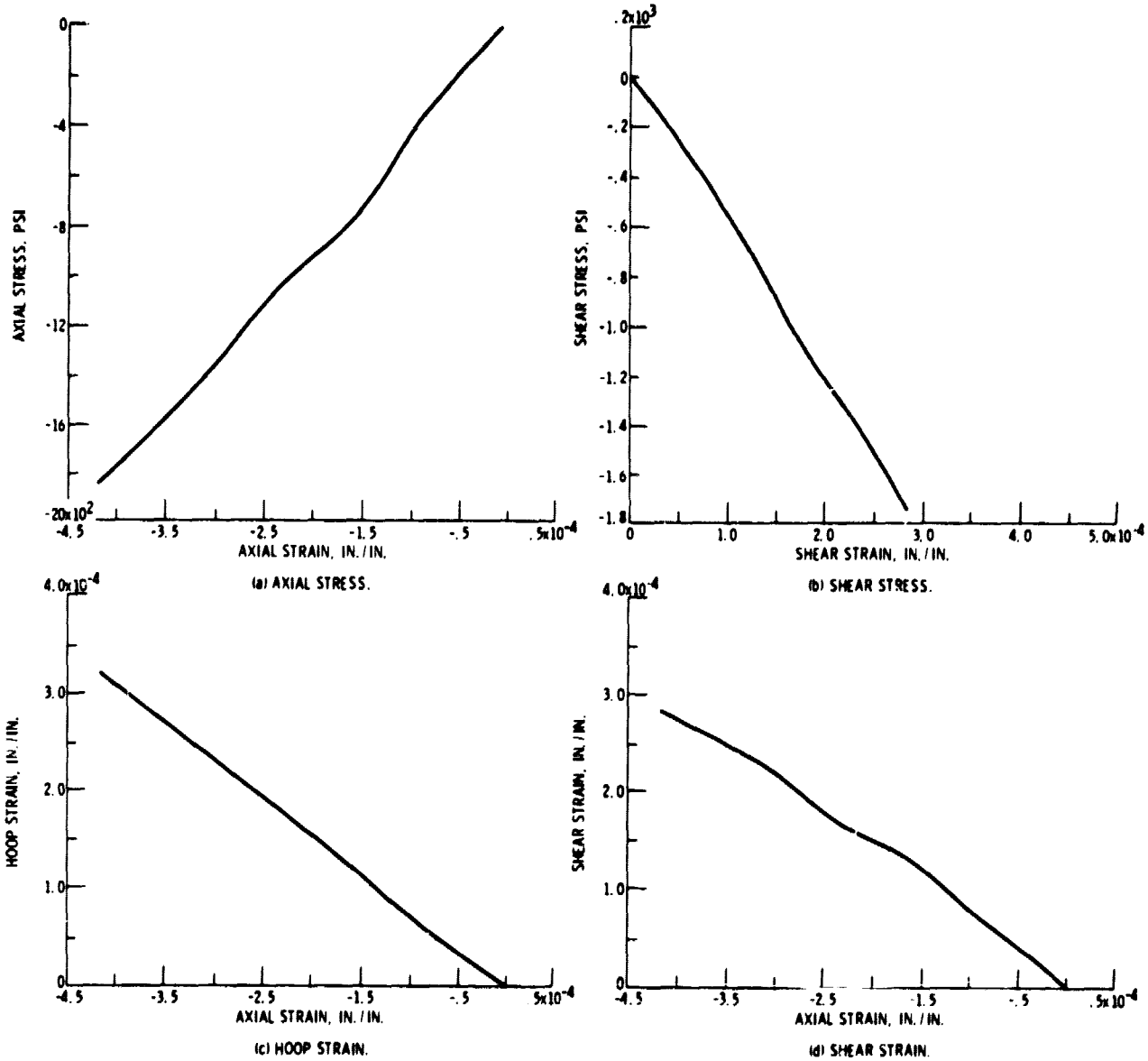

Figure 11. - Stress-strain and strain-strain curves for a thin composite tube subjected to combined stress ratio (-1:0:-1). $\left[\pm 45\right]_2\Big]_s$ boron/epoxy. 0.50 fiber volume ratio.

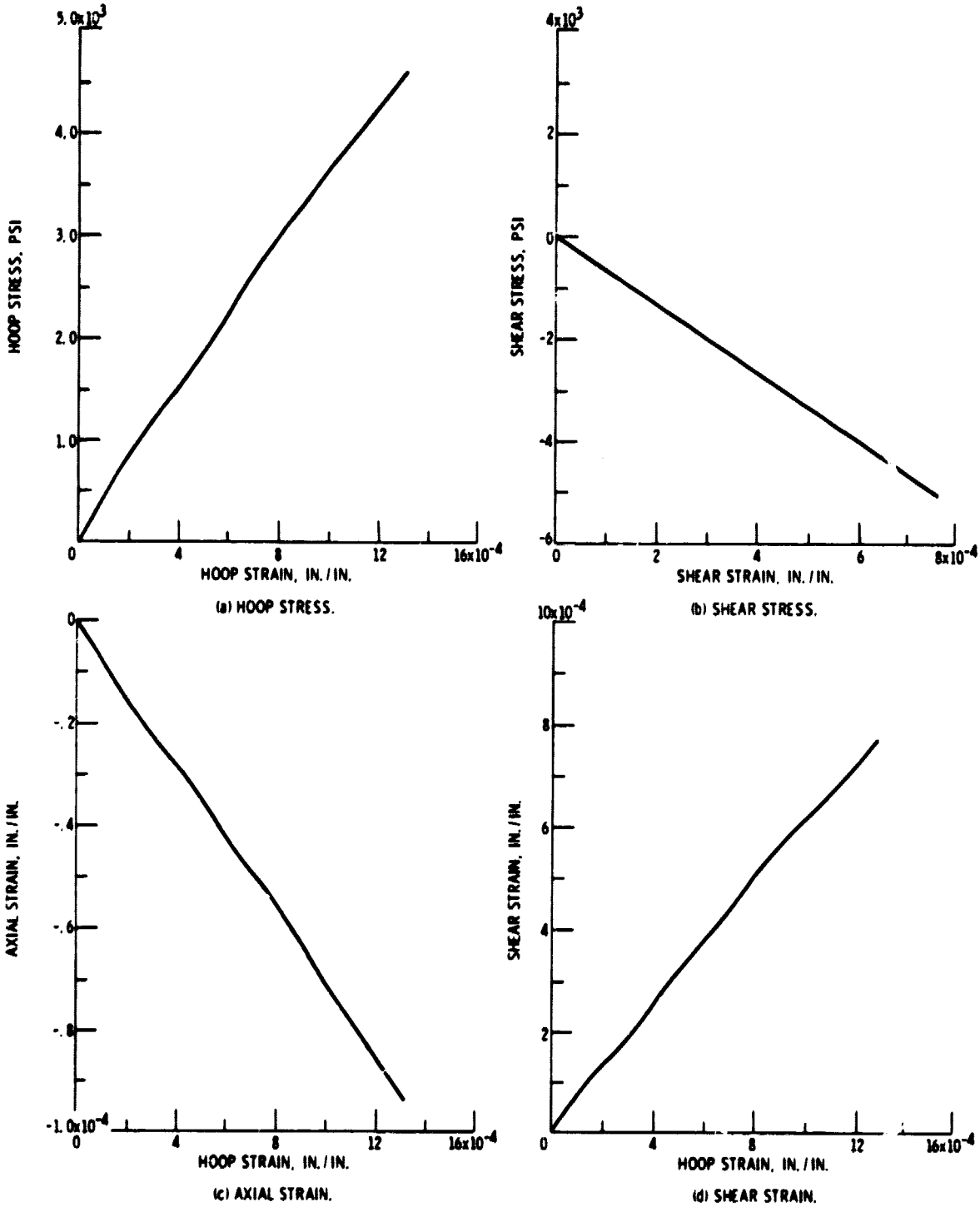

Figure 12. - Stress-strain and strain-strain curves for a thin composite tube subjected to combined load stress ratio (0:1:-1). $\left[(\pm 45)_2\right]_s$ boron/epoxy, 0.50 fiber volume ratio.

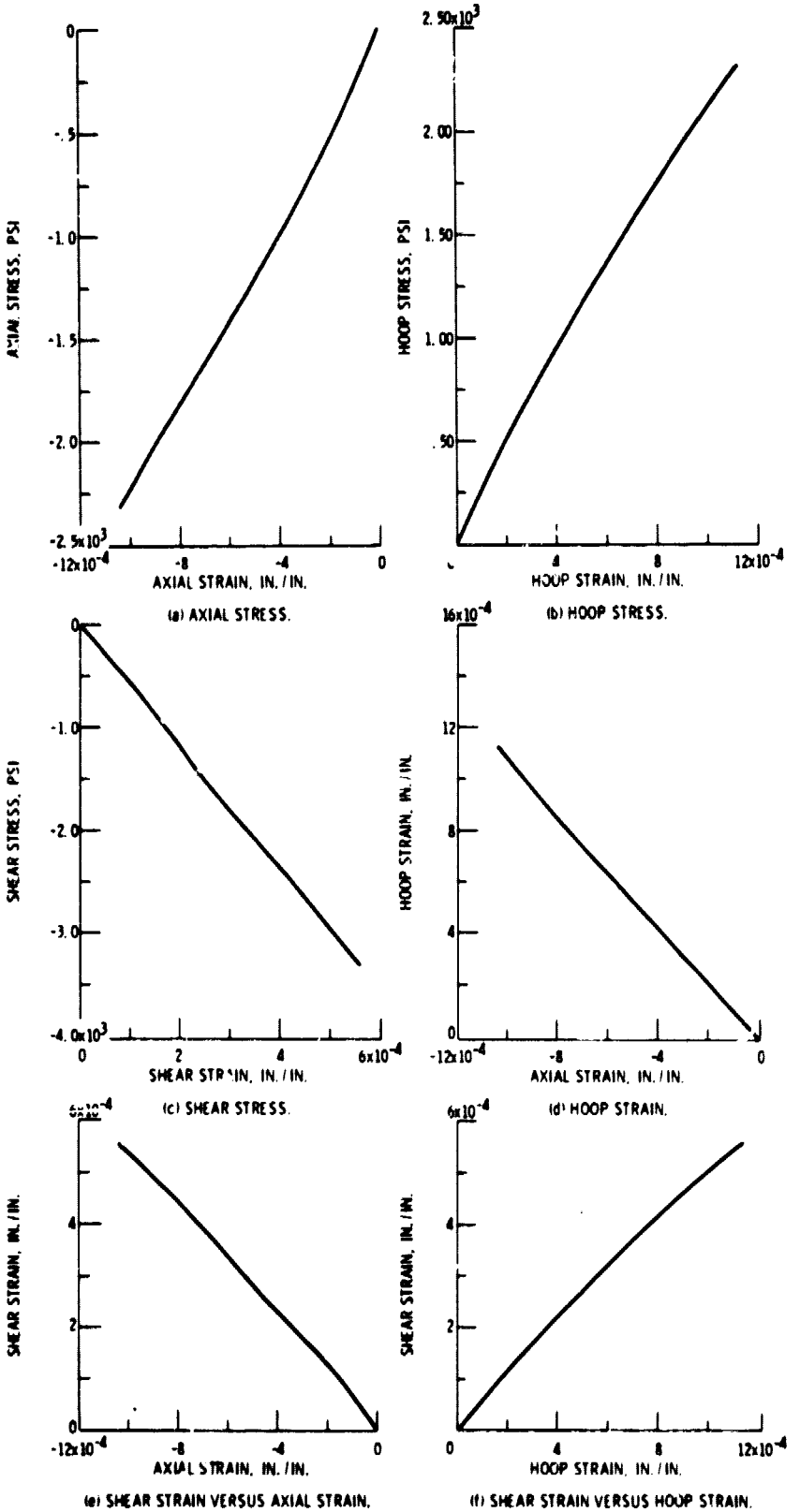

Figure 13. - Stress-strain and strain-strain curves for a thin composite tube subjected to combined load stress ratio (-1:1:-1). $[(\pm 45)_2]_s$ boron/epoxy, 0.50 fiber volume ratio.

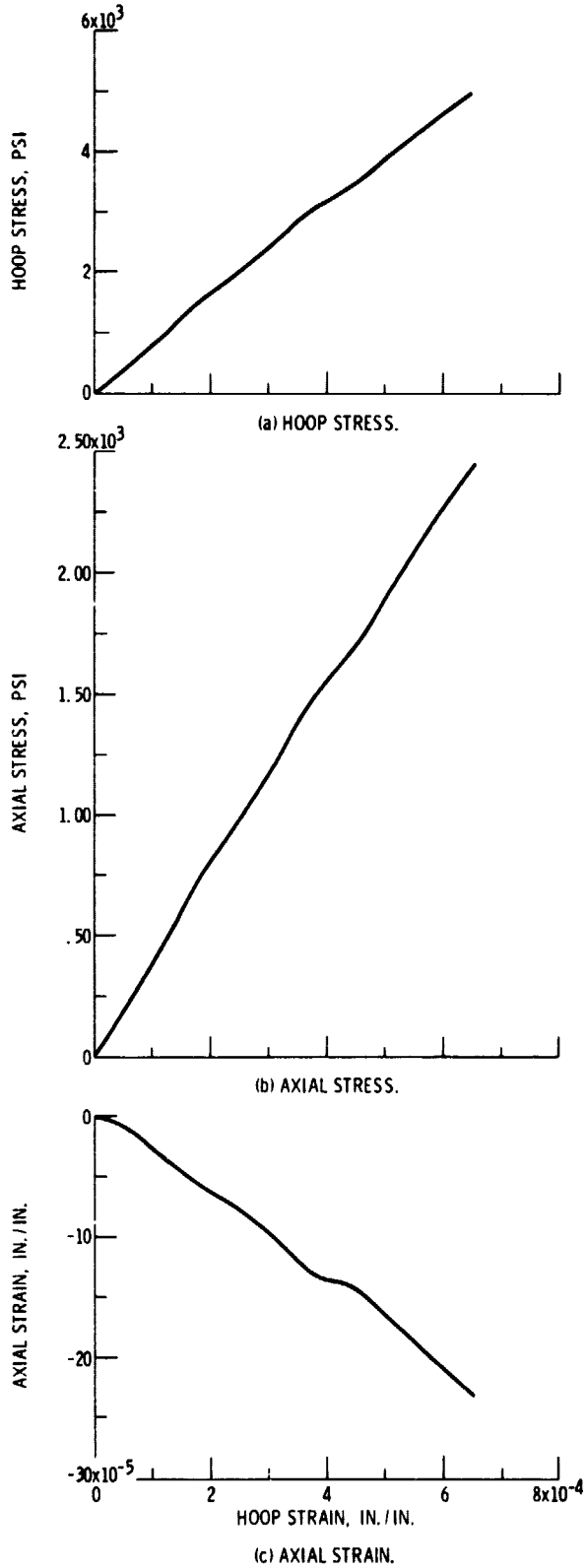

Figure 14 - Stress-strain and strain-strain curves for a thin composite tube subjected to internal pressure (1:2:0). $[(\pm 45)_2]_S$ boron/epoxy, 0.50 fiber volume ratio.

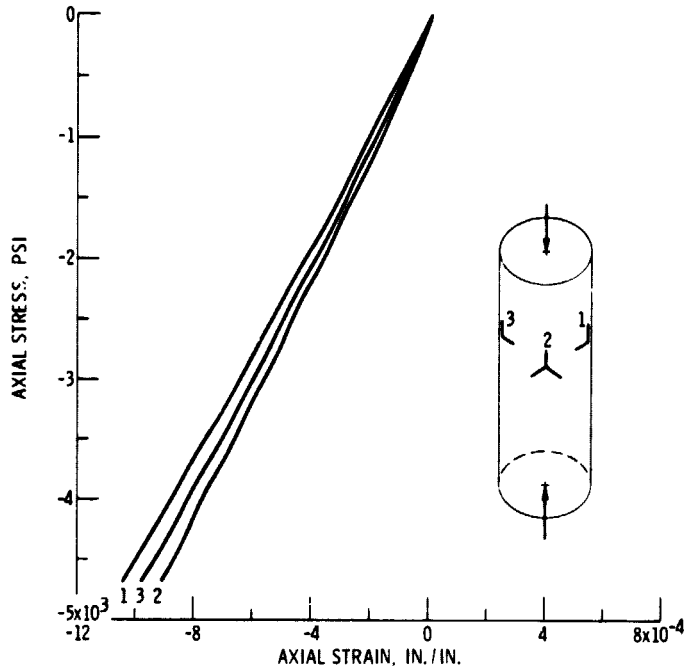

(a) AXIAL STRESS.

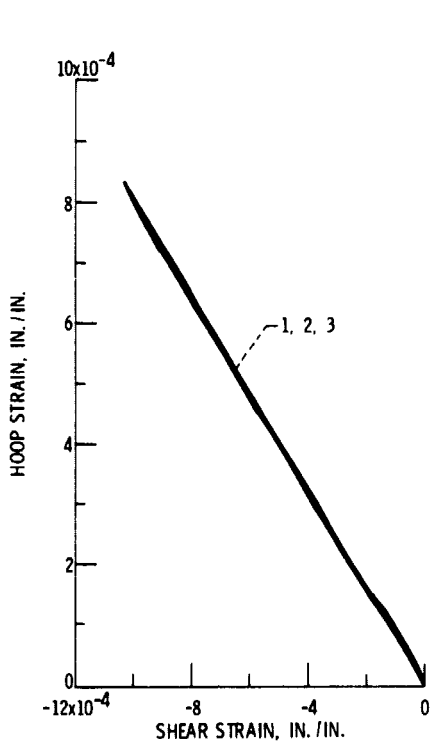

(b) HOOP STRAIN.

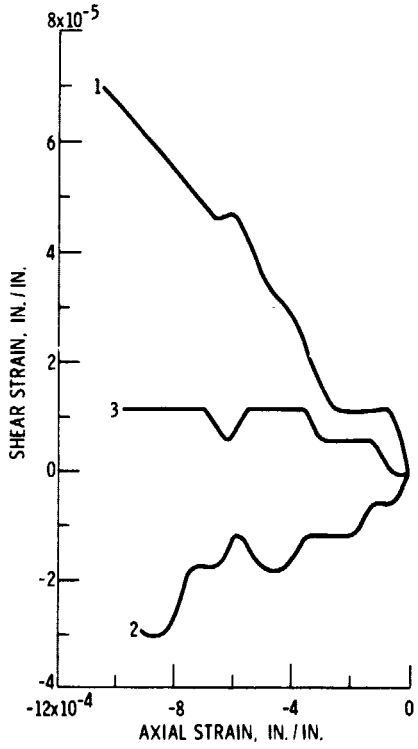

(c) SHEAR STRAIN.

Figure 15. - Stress-strain curves for a thin composite tube subjected to axial compression. $[(\pm 45)_2]_s$ boron/epoxy, 0.50 fiber volume ratio.

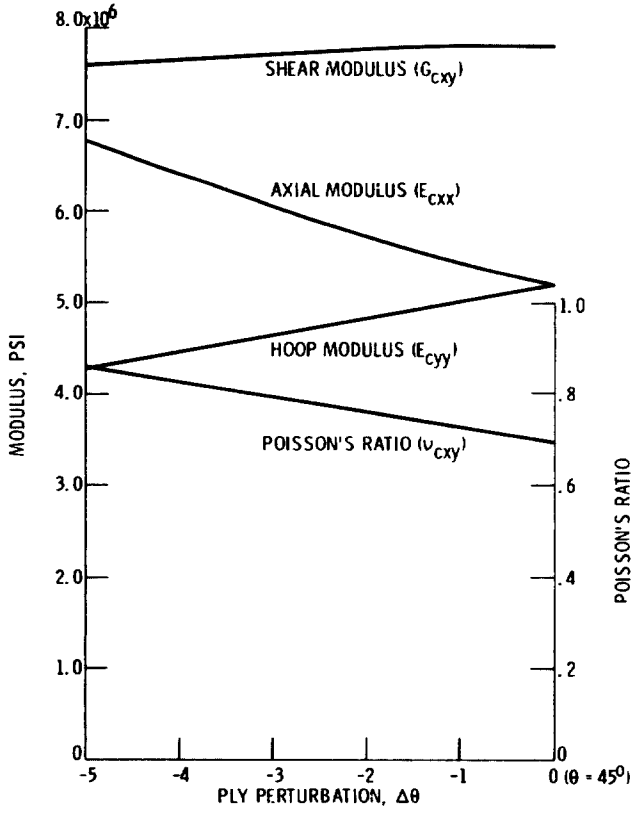

Figure 16. - Theoretical variation of composite elastic properties with small perturbations about 45^0 for a boron/epoxy composite $[(\pm 45^0)_2]_s$ at 0.5 fiber volume ratio, zero voids and ply shear modulus = 1.54×10^6 psi.

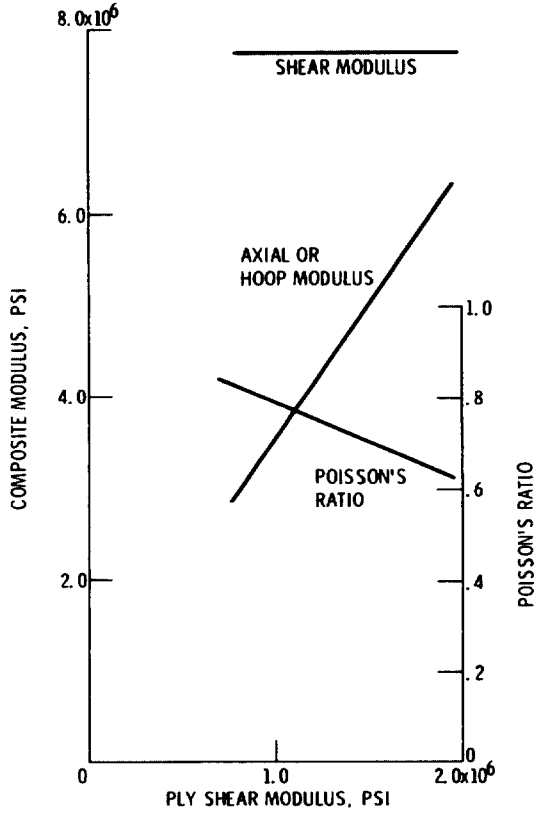

Figure 17. - Theoretical variation of composite elastic properties with ply shear modulus for a boron/epoxy composite $[(\pm 45)_2]_s$ at 0.5 fiber volume ratio and zero voids.